Surface anchoring structure of a liquid crystal monolayer studied via dual polarization interferometry

Osbert Tan and Graham H. Cross[*]

Department of Physics, University of Durham, South Road, Durham, DH1 3LE, United Kingdom
(Received 8 October 2008; published 18 February 2009)

The self-organization of liquid crystal molecules of 4-*n*-pentyl-4′-cyanobiphenyl (5CB) forming an oriented monolayer by condensation from the vapor phase onto a silicon oxynitride surface has been observed using the evanescent wave dual slab waveguide dual polarization mode interferometry (DPI) technique. Two distinct stages to the layer formation are observed: After the formation of a layer of molecules lying prone on the surface, further condensation begins to densify the layer and produces a gradual mutual alignment of the molecules until the fully condensed, fully aligned monolayer is reached. At this limit the full coverage 5CB monolayer on this surface and at a temperature of 25 °C, is found to be anchored with an average molecular axis polar angle of $56 \pm 1°$ and with a measured thickness of 16.6 ± 0.5 Å. These results are in reasonable agreement with the molecular dimensions provided by molecular models. The apparent precision and accuracy of these results resolves some wide disparity between earlier studies of such systems. Previous difficulties in determining optogeometrical properties of such ultrathin birefringent films using ellipsometry or in the need for complex modeling of the film layer structure using x-ray reflectivity are overcome in this instance. We provide a technique for analyzing the dual polarization data from DPI such that the bulk refractive index values, when known, can be used to determine the orientation and thickness of a layer that is on the nanometer or subnanometer scale.

I. INTRODUCTION

The dual slab waveguide interferometer [1] is becoming a standard tool in the laboratory for the determination of the optogeometrical properties of biological and other physicochemical ultrathin films. Widely applied to the investigation of the structure and affinity binding characterization of biological material captured from water-based flowing buffers, the optogeometrical (refractive index and thickness) properties resolved from the dual polarization implementation of the interferometer are highly accurate [2,3]. This is due usually to the low layer birefringence inherent in the systems studied. However, as has been observed a number of times, many important layers of interest have substantial birefringence and models assuming uniform (through the layer thickness) and isotropic structure will lead to errors in the analysis [4,5]. Provided part of the information required is available from other methods, however, such highly birefringent layers can be analysed successfully. In the case of the dual polarization interferometer (DPI), one such application of this has been in the determination of the birefringence of supported lipid bilayers (as cell membrane mimics) where a reliable value for the bilayer thickness, determined from neutron scattering, is used as input data [6].

Whereas the maximum birefringence measured for lipid bilayers in [6] is on the order of around 0.02, some layer forming systems, such as liquid crystals, may have maximum birefringence values one order of magnitude higher [7]. Furthermore, while the intermolecular forces between lipid molecules dominate the bilayer formation on solid surfaces, the interaction between the surface and the molecules is very much more influential in the case of liquid crystal layers forming at the surface. For this reason, the growth of such layers is very much more complicated and there is only slowly growing understanding of the effect of the surface properties on the morphology of the first few layers of liquid crystal. The alignment of a nematic liquid crystal (NLC) at the interfacial surface region is of particular importance, since the surface induced alignment is essential for the operation of many NLC devices. The anchoring of NLC at solid substrates can be classified into several types depending on the morphology and properties of the substrate surface. Typically, an isotropic clean glass, or similar, surface induces planar anchoring [8]; a NLC on a unidirectionally rubbed polymer surface prefers a tilted anchoring [9] and a surface upon which is deposited molecules with long aliphatic chains (such as in some Langmuir-Blodgett films) may sometimes produce homeotropic (vertical) alignment because of interaction between the NLC short aliphatic chain and the surface bound aliphatic chains [10,11]. In the azimuthal aspect, the isotropy or anisotropy of the azimuthal orientation is also directed by that of the substrate surface [2]. The molecular-scale details of surface anchoring effects are therefore far from being understood due to the complication of the anisotropic interactions between the solid surface and the NLC molecules.

We set out in this paper to show how DPI may be used to determine the average molecular orientation in a liquid crystal monolayer deposited by thermal evaporation provided, as is the case, that there is prior knowledge of fundamental physical and optical properties, namely, molecular dimensions and bulk phase refractive index values. We validate and provide a method of interpreting the raw data from DPI, namely, the phase changes in the probe waveguide modes in each of the two polarization states, to give an indication of

---

*g.h.cross@durham.ac.uk

the polar and surface azimuthal alignment of the molecules in ultrathin layers such as these. The method will be applicable to any layer material system of any birefringence that is amenable to DPI analysis and for which optical and geometrical data is available.

In the experimental verification of our method we provide a report of vapor phase deposition studies using DPI. We report an optical anisotropy analysis of a monolayer 4-n-pentyl-4′-cyanobiphenyl (5CB) film grown by thermal evaporation onto a silicon oxynitride (SiO_xN_y) substrate which acts as the waveguide layer in the dual slab waveguide interferometer. Adsorbed 5CB layers are considered as an ultrathin interfacial film within which the optical refractive index anisotropy is strongly correlated to, and evolves with, the density and thickness of the layers. The scale of the film thickness (t) possessing this surface anchoring anisotropy is expected to be smaller than 200 Å, which is equivalent to about 12 layers of 5CB where the molecular length is 17 Å.

It will be apparent that where at least three parameters (thickness and two orthogonal refractive index values) are to be resolved from data that comprise only two independent measurements (waveguide mode phase changes in two orthogonal polarization states), some extra assumptions must be introduced [5,6]. In the first part of the present work, we introduce some fundamental aspects of NLC molecular optogeometrical and layer geometry properties that will justify the assumptions made later. We then set out a complete analysis of the multiparameter space within which the experimental data can be interpreted. The pairs of polarization state data, taken as ratios, can then be mapped onto ranges of structural possibilities within the whole space. Within these ranges, some specific structural motifs can be considered high probabilities given other known aspects of the substrate and material.

II. BACKGROUND AND THEORY OF NLC SURFACE LAYERS

A. Prior work

The anchoring effect of NLCs or smectic LCs on solid substrates has been extensively studied experimentally by surface second harmonic generation [12,13], polarized absorption spectroscopy [14], ellipsometric [15,16], x-ray reflectivity [17], and neutron reflection [18] methods for both thermally evaporated LC films and spreading droplets. Theoretical work has also revealed the orientation behaviour to be expected of ultrathin LC layers adjacent to their anchoring surface [19,20]. There is general agreement in both experimental and theoretical work that the anchoring profile of nCB molecules on untreated, clean solid surfaces can be described in terms of a metastable precursor film which is made up of a contact monolayer covered with an interdigitated bilayer. The existence of this trilayer structure is also observed in the form of Langmuir films settled at the water-air interface for 8CB molecules [21], which gives further support for the trilayer model proposed on solid surfaces. The first layer of this system is the subject of the present study. In previous work it has been shown that a monolayer of evaporated 5CB on plain silica is oriented at 63° to the surface
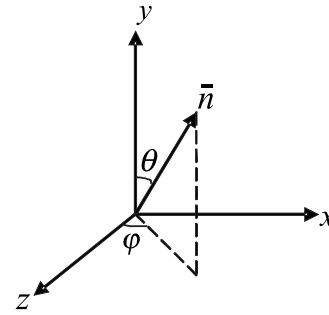

FIG. 1. NLC director, $\bar{n}$ in the experimental coordinate reference frame.

normal [15] (recalculated as 62° by us according to the equation given), but with uncertainty added from our examination of Fig. 2(b) in that report, an error of ±4° might be applied to this value. The molecular polar angle in monolayers on silica (usually the native oxide layer of a silicon wafer, or alternatively on fused silica) of the closely related LC molecule 8CB has also been determined to be 67°, 74°, or 57°, depending on different measurement methods [12,13,17]. Furthermore, contradictory evidence from scanning polarization force microscopy [22] gives the total monolayer thickness to be 8 Å interpreted as comprising the cyanobiphenyl system at 90° to the surface normal with the aliphatic tail at 60° (i.e., 30° to the surface plane). This wide range indicates the difficulties inherent in such measurements as well as the problems of transferring the interpretations of experimental data between different methods. In the present work, we use an experimental technique that overcomes many of the obstacles and limitations of previously used techniques and show that reliable data interpretations can be made with only the minimum of assumptions, primarily that the bulk refractive index values of the material may be applied to ultrathin surface bound layers.

B. Layer permittivity properties

The anisotropic refractive index of a NLC layer with average director field $\bar{n}$ in the experimental coordinates can be obtained via coordinate transformation of the dielectric tensor of NLC molecules [23]. The intrinsic dielectric tensor of the uniaxial NLC molecule is set to be

$$
\begin{pmatrix}
n_o^2 & & \\
& n_o^2 & \\
& & n_e^2
\end{pmatrix}
$$

with ordinary refractive index n_o and extraordinary refractive index n_e perpendicular to, and along, the molecular axes, respectively. The tilted molecular ensemble with average polar and azimuthal angles θ and φ (shown in Fig. 1) will have new dielectric constants in the x, y, and z directions, given as

$$
n_z^2 = \frac{1}{2}[2n_o^2 + (n_e^2 - n_o^2)\sin^2\theta] + \frac{1}{2}(n_e^2 - n_o^2)\sin^2\theta\cos 2\varphi,
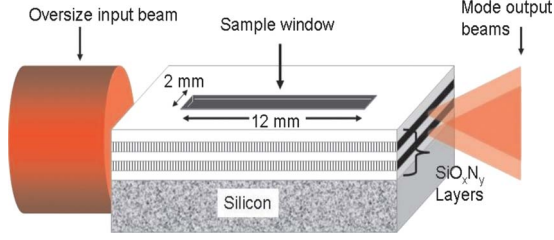$$

(1)

FIG. 2. (Color online) Schematic dual slab waveguide interferometer structure. Hatched layers are confinement layers. An oversized input beam illuminates the whole end facet. Emergent beams form an interference pattern on the linear photodiode array (not shown.)

$$n_x^2 = \frac{1}{2}[2n_o^2 + (n_e^2 - n_o^2)\sin^2\theta] - \frac{1}{2}(n_e^2 - n_o^2)\sin^2\theta\cos 2\varphi, \tag{2}$$

$$n_y^2 = n_e^2 - (n_e^2 - n_o^2)\sin^2\theta. \tag{3}$$

As for the untreated, pure, clean, SiO_xN_y substrate, we generally consider it to be isotropic in the azimuthal plane due to its amorphous bulk structure. The NLC molecules adsorbed on this isotropic surface will then assume degenerate tilt or planar anchoring. We thus only calculate the xz plane average refractive index with no preferential azimuthal angle for the adsorption layers, such that

$$\langle n_z^2 \rangle = \langle n_x^2 \rangle = \frac{1}{2}[2n_o^2 + (n_e^2 - n_o^2)\sin^2\theta], \tag{4}$$

$$\langle n_y^2 \rangle = n_e^2 - (n_e^2 - n_o^2)\sin^2\theta, \tag{5}$$

where we use $\langle\cos 2\varphi\rangle = 0$.

The monolayer film on this surface will exhibit a polar angle characteristic of the first layer of the characteristic "three-layer" model accepted for such systems. We can therefore treat the whole layer as having uniaxial symmetry.

III. THEORY OF THE DUAL SLAB WAVEGUIDE

The dual slab waveguide interferometer used to detect the optical anisotropy of the adsorbed films simply comprises a five-layer dielectric stack on the semiconductor wafer surface. The device is fabricated on a silicon substrate with silicon oxynitride dielectric layers, as shown in Fig. 2.

The method of operation has been extensively described before [24]. Input light at 632.8 nm and switched alternately at 50 Hz into each of two orthogonal polarization states, excites equally the transverse electric (TE, z polarized input field) and transverse magnetic (TM, y polarized input field) single modes of the dual slab structure. The output interference image from the device can be decoded to give the phase variations in the upper waveguide mode field as a result of material deposited on the upper waveguide surface (layer 4) in the window region. These phase variations, associated with the density and thickness of the adsorbing layer are calculated in terms of the perturbation rate of the effective

index of the upper guiding waveguide mode. At the device output plane, the relative phase position of the upper and lower waveguide modes for TE is

$$\phi_E = k_0 N_{E4c}(l_t - l) + k_0\int_0^l N_E(x)dx - k_0 N_{E2}l_t, \tag{6}$$

where N_{E4c} is the TE mode effective index of the mode confined to layer 4 in the region with cladding (layer 5); $N_E(x)$ is the effective index of the mode confined to layer 4 in the window region as a function of position; N_{E2} is the lower waveguide mode effective index. The length of the chip and that of the window region are denoted l_t and l, respectively, and k_0 is the free space wave number. Similarly, for the TM phase variation,

$$\phi_M = k_0 N_{M4c}(l_t - l) + k_0\int_0^l N_M(x)dx - k_0 N_{M2}l_t, \tag{7}$$

where N_{M4c}, $N_M(x)$, and N_{M2} have the same meaning as the counterparts in the TE mode. Equations (6) and (7) can be simplified into

$$\phi_E = C_E + k_0\int_0^l N_E(x)dx, \tag{8}$$

$$\phi_M = C_M + k_0\int_0^l N_M(x)dx, \tag{9}$$

where we define phase constants $C_E = k_0 N_{E4c}(l_t - l) - k_0 N_{E2}l_t$ and $C_M = k_0 N_{M4c}(l_t - l) - k_0 N_{M2}l_t$, which are irrelevant to the NLC deposition.

During the growth of the film there is the problem that the sensing waveguide effective index is variable along the propagation direction. The layer may form in an irregular way rather than by a completely uniform, layer-by-layer process. Islands comprising multiple layers (presumably including the trilayer motif, see above) may transitorily form and then disperse during the deposition, for example. The observation of the well defined terrace formed by a trilayer of NLC between the bulk region and monolayer region of a spreading droplet suggests that this is possible. At any time during deposition therefore, the single polarization measurement, taken by integrating the effective index changes along the path length, thus represents the average layer properties reflected in a notional layer thickness t' and refractive index n'. We may represent these averages as $t' = \int_0^l[t(x)dx]/l$ and $n' = \int_0^l[n(x)dx]/l$ where $t(x)$ and $n(x)$ are the actual thickness and index distributions along the window path of length l.

The average thickness is measured, of course, independent of the mode polarization state but the refractive index is representative of the average projection of the molecular dielectric tensor components onto the experimental reference frame as embodied in Eqs. (4) and (5). As such, we can form two equations that represent the enlargement of the mode effective index that includes the average refractive indices in each polarization state n_E' and n_M' as follows:

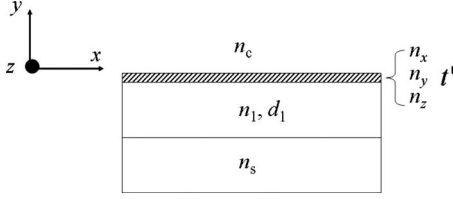$$N_E = a(n_E', t')t' + N_E^0, \tag{10}$$

FIG. 3. Waveguide configuration and optogeometrical parameters of sensing guiding layer and the NLC adsorption layer

$$N_M = b(n'_M, t')t' + N_M^0, \qquad (11)$$

where N_E^0 and N_M^0 are the sensing waveguide effective indices of TE and TM modes for the bare surface before deposition and a and b are what we call the TE and TM perturbation rates to the waveguide effective index due to the development of the adsorption layers. These parameters are functions of the average observed refractive index and average observed thickness of the layer. Note that the average refractive indices given in (10) and (11) are related to the indices given in (4) and (5), respectively. Thus at a certain time when the NLC films have a certain average anchoring alignment, the parameters a and b contain information about the polar angle of films.

Equations (8) and (9) can now be transformed into

$$\phi_E = C_E + k_0 N_E^0 l + k_0 l a t' = \phi_E^0 + k_0 l a t', \qquad (12)$$

$$\phi_M = C_M + k_0 N_M^0 l + k_0 l b t' = \phi_M^0 + k_0 l b t', \qquad (13)$$

where ϕ_E^0 and ϕ_M^0 are defined as the initial TE and TM phases, before NLC deposition.

Furthermore, the TE and TM phase change ratio [dividing Eqs. (12) and (13)] is simply the ratio of the two perturbation rates,

$$\frac{\phi_E - \phi_E^0}{\phi_M - \phi_M^0} \equiv \frac{\Delta\phi_E}{\Delta\phi_M} = \frac{a}{b}, \qquad (14)$$

where the TE phase change $\Delta\phi_E$ and TM phase change $\Delta\phi_M$ can be experimentally measured by the shift of the modal interference fringes. If the perturbation ratio is only the function of average molecular orientation (i.e., parameters a and b are constant with thickness for any constant orientation), the NLC layer anchoring orientation and dynamics can be detected by the TE and TM phase change ratio in real time as the phase changes are recorded.

To obtain the effective index perturbation rates a and b, a standard numerical method is used to calculate the sensing guiding layer effective index at any given polar angle and over a range of thicknesses of adsorbed layer. The multilayer transfer matrix method [25] is used to efficiently evaluate the effective index of the four-layer waveguide structure, as shown in Fig. 3.

Therefore the transfer matrix product for TE mode is

$$M_{\text{TE}} = \begin{pmatrix} m_{11} & m_{12} \\ m_{21} & m_{22} \end{pmatrix} = \begin{pmatrix} \cos(\alpha_1 d_1) & -\dfrac{1}{\alpha_1}\sin(\alpha_1 d_1) \\ \alpha_1 \sin(\alpha_1 d_1) & \cos(\alpha_1 d_1) \end{pmatrix}$$

$$\times \begin{pmatrix} \cos(\alpha_m t') & -\dfrac{1}{\alpha_m}\sin(\alpha_m t') \\ \alpha_m \sin(\alpha_m t') & \cos(\alpha_m t') \end{pmatrix}, \qquad (15)$$

where $\alpha_1 = k_0\sqrt{n_1^2 - N_E^2}$ and $\alpha_m = k_0\sqrt{n_z^2 - N_E^2}$ with N_E the effective index of the TE mode. The associated eigenvalue equation is

$$F(N_E) = \alpha_s m_{11} + \alpha_c m_{22} - m_{21} - \alpha_s \alpha_c m_{12} = 0, \qquad (16)$$

where $\alpha_s = k_0\sqrt{N_E^2 - n_s^2}$ and $\alpha_c = k_0\sqrt{N_E^2 - n_c^2}$. The solution of Eq. (16) corresponds to the effective refractive index of the TE mode.

Similarly, the effective index for the TM mode can also be numerically obtained in the same way. Thus the transfer matrix product is

$$M_{\text{TM}} = \begin{pmatrix} m_{11} & m_{12} \\ m_{21} & m_{22} \end{pmatrix} = \begin{pmatrix} \cos(\alpha_1 d_1) & -\dfrac{n_1^2}{\alpha_1}\sin(\alpha_1 d_1) \\ \dfrac{\alpha_1}{n_1^2} \sin(\alpha_1 d_1) & \cos(\alpha_1 d_1) \end{pmatrix}$$

$$\times \begin{pmatrix} \cos(\alpha_m t') & -\dfrac{n_x^2}{\alpha_m}\sin(\alpha_m t') \\ \dfrac{\alpha_m}{n_x^2} \sin(\alpha_m t') & \cos(\alpha_m t') \end{pmatrix}, \qquad (17)$$

where $\alpha_1 = k_0\sqrt{n_1^2 - N_M^2}$ and $\alpha_m = (n_x/n_y)k_0\sqrt{n_y^2 - N_M^2}$ with N_M the effective index of the TM mode. The eigenvalue equation thus is

$$F(N_M) = \frac{\alpha_s}{n_s^2}m_{11} + \frac{\alpha_c}{n_c^2}m_{22} - m_{21} - \frac{\alpha_s \alpha_c}{n_s^2 n_c^2}m_{12} = 0, \quad (18)$$

where $\alpha_s = k_0\sqrt{N_M^2 - n_s^2}$ and $\alpha_c = k_0\sqrt{N_M^2 - n_c^2}$.

The TE and TM index perturbation rates a and b are acquired via the linear regression, in terms of least squares, of the TE and TM effective indices calculated in increasing adsorption layer thickness, t' (up to an equivalent of ten NLC molecular layers).

IV. SIMULATION RESULTS: UNIAXIAL SYSTEMS

The refractive indices of 5CB are well-documented properties and at the wavelength of the experiments ($\lambda_0 = 632.8$ nm) and at the experimental temperature (23 °C) we use the dispersion equations given by Li and Wu [7] and use $n_o = 1.527$, $n_e = 1.712$. As provided in Eqs. (4) and (5) (shown plotted in Fig. 4), in the azimuthal-degenerate anchoring condition, the azimuthal and polar refractive indices for any thickness of adsorbed NLC layer are only a function of the average polar tilt angle θ and can be used as input data to the waveguide eigenvalue equations.

In our waveguide structure, the TE refractive index is that measured along the z axis of Fig. 3; thus, $n_{\text{TE}} = n_z$. The TM
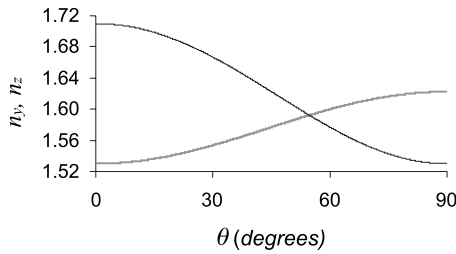
FIG. 4. Layer refractive indices (n_z, gray line; n_y, black line) of degenerate anchoring NLC layers as a function of the polar tilt angle of molecules

refractive index is slightly more complicated in that there are components of the mode electric field along both the y and x axes and their relative proportion is a function of the effective index. However, for azimuthal degeneracy we may assign $n_x = n_z$ for use in Eq. (17).

The thickness $d_1 = 1.0165$ μm and index $n_1 = 1.522$ of the waveguide confinement layer are determined by an experimental calibration procedure [26]. The substrate index is taken to be $n_s = 1.480$ and the cladding index $n_c = 1.000$.

We thus calculate both the TE and TM perturbation rates a and b of the waveguide effective index as a function of increasing effective thickness t' of the NLC adsorption layers. We find that a and b are accurately described by linear gradients of effective index versus thickness. We are interested in the first few nanometers of adlayer but the linearity remains valid up to at least 180 nm for the wavelength and waveguide structure we have here.

As Fig. 5(a) shows, the TE perturbation rate shows a large variation with increasing θ, whereas the TM rate shows a smaller range and is essentially constant. This difference in sensitivity is in part due to the lower confinement of the TM mode in the system. The ratio of TE and TM perturbation rates ($r \equiv a/b$) shows monotonic behavior, ranging from 0.806 to ~0.978, corresponding to homeotropic ($\theta \sim 0°$) and homogeneous ($\theta \sim 90°$) anchoring of the NLC thin film, respectively. Note that the ratio passes a maximum at near $\theta = 83°$.
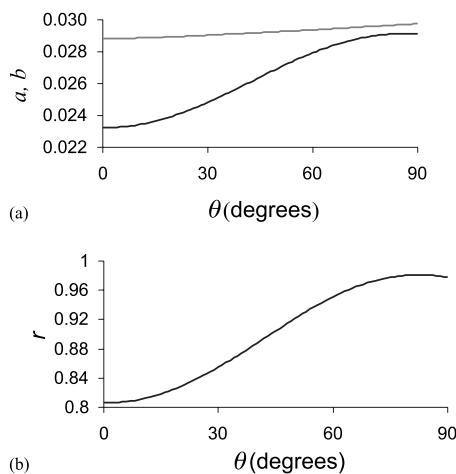

(a)

(b)

FIG. 5. (a) TE and TM perturbation rates (a, black line; b, gray line) versus molecular tilt angle. (b) Ratio $r = a/b$ versus molecular tilt angle.
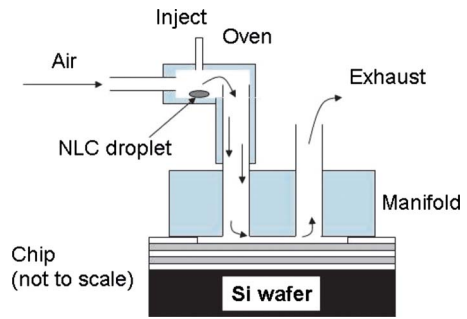

FIG. 6. (Color online) Schematic diagram of the vapor flow arrangements for thermal evaporation of the NLC.

V. EXPERIMENTAL METHOD

The dual slab waveguide sensor chip is cleaned by soaking in "piranha" solution (50:50 v/v concentrated sulfuric acid and 30% hydrogen peroxide) for 10 min, followed by rinsing in deionized water then dried with nitrogen gas. It is then further cleaned in an O_2 plasma, and experiments are conducted within 2 h after removal from the plasma chamber. Typical surfaces prepared in this way exhibit water drop contact angles below 5° (the resolution of our experiment) as determined by the sessile drop method, indicating an absence of hydrocarbon contaminants.

The cleaned sensor chip is clamped inside a dual-zone temperature controlled housing providing temperature control to ± 10 mK. The temperature of the chip is set to be 25 °C. The window region of the chip is exposed to a flow of air that can be controlled by valves and a simple small aquarium pump. The flow passes through a small copper heated oven into which may be injected 5–6 μl of liquid crystal. The oven is directly connected to the input and output manifold of the chip housing which is fabricated from a thermally insulating material (Tufnol) and which is pressed onto a flat rubber gasket lying on the chip surface inside the housing, as shown in Fig. 6.

After injection the liquid crystal is heated up to 90 °C, and the flow valve is regulated to allow the air-diluted liquid crystal vapor to flow gently through the manifold and over the sensor chip. The flow rate is adjusted by monitoring the phase changes recorded as the liquid crystal begins to condense on the chip surface.

VI. EXPERIMENTAL RESULTS AND DISCUSSION

The recorded TE and TM phase change data calculated via discrete Fourier transform algorithm from the modal interference fringe pattern is displayed in Fig. 7(a). As shown in the graph, the gradual increase of phase in both TE and TM modes indicates liquid crystal adsorption on the waveguide surface and the rise of the effective indices by the addition of NLC layers. The final plateau region corresponds to the closure of the valve, and NLC deposition is stopped. During the data collection we also measure the fringe contrast or "visibility" [see Fig. 7(b)]. This parameter depends upon the output optical power balance between the upper and lower waveguide modes. It can provide very clear evidence
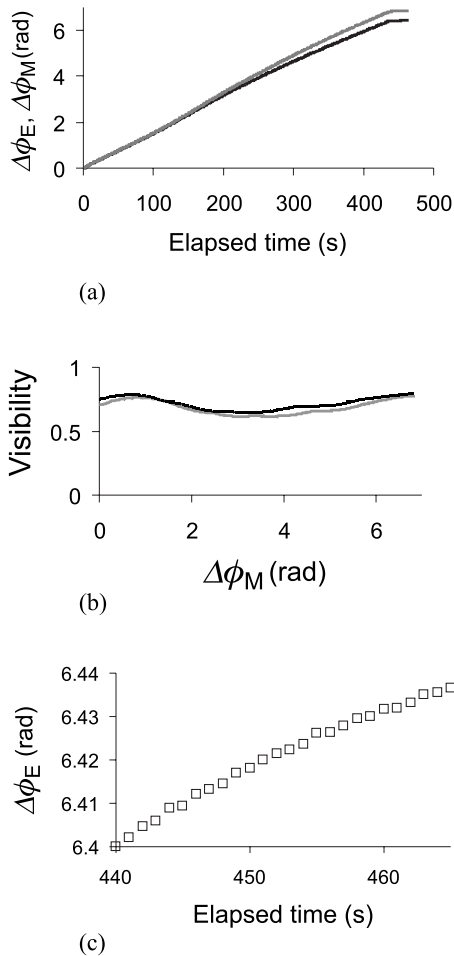
(a)

(b)

(c)

FIG. 7. (a) TE (black line) and TM (gray line) mode phase changes during the NLC deposition. The valve is closed at 440 s. (b) TE and TM fringe contrast as a function of NLC deposition showing no overall loss of contrast over the full deposition range. The curvature exhibited is typical of static image defect contributions, which are 2π cyclical. Such defects can give rise to cyclical phase errors, but note that the TE and TM defect contributions are in phase and therefore contribute very little error to the measured phase change ratio. (c) Detail of experimental noise showing the TE phase change measured with the valve closed after the deposition is concluded. The upward drift in the phase response is presumably due to liquid crystal deposition from the stagnant air space above the sample.

of optical power loss from the upper waveguide mode during experiments [27] and would indicate any dewetting and drop formation during the deposition cycle. Such events will lead to loss of confinement and/or interface scattering of the upper waveguide mode. This evidence strongly suggests therefore that the deposition is conducted sufficiently slowly that the liquid crystal can completely wet the surface rather than condensing into its bulk phase [28]. The inherent low noise in the system is seen by examining the data in the region of the data where the valve has been switched off [Fig. 7(c)]. Each data point is recorded with a precision of ± 0.001 rad. This noise, which is probably largely thermal in origin, allows us to formally set the precision of the ratio of phase changes to around ± 0.0014.
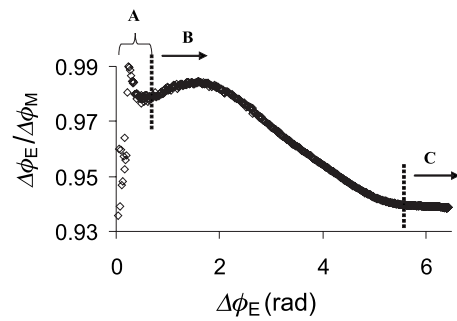

FIG. 8. TE and TM phase change ratio $(\Delta\phi_E/\Delta\phi_M)$ plotted against the TE phase change, which indicates the mass of deposited NLC molecules.

The ratio of the phase changes up to the point of valve closure is shown in Fig. 8 where key regions and demarcation points in the deposition path are noted. The great power provided for structural interpretation by taking the *ratio* of experimental phase changes is evident in the marked nonuniformity shown here compared to the rather monotonic behavior of the phase changes if taken by themselves [Fig. 7(a)]. The following proposals are made for the mechanism of layer formation by reference to regions *A*, *B*, and *C* of Fig. 8 and given in greater detail and with a deposition model in Figs. 9 and 10.

A. Discussion of the deposition regions

1. Region A

During the initial stages of deposition, molecules find surface anchoring sites at random and adopt a range of azi-
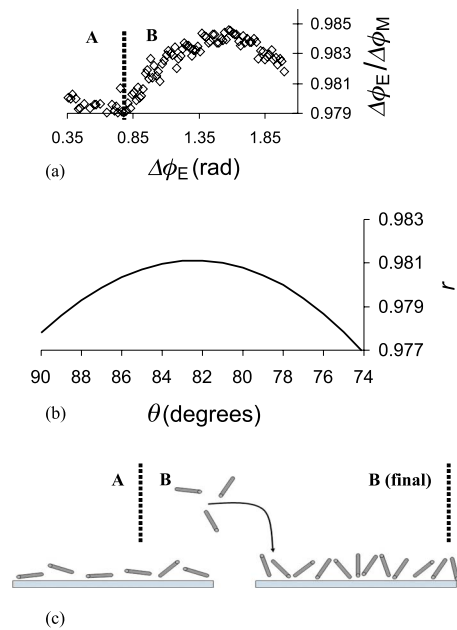

(a)

(b)

(c)

FIG. 9. (Color online) (a) Detail of the experimental data at the start of the reorientation region. (b) Detail of the theoretically determined perturbation rate ratio modeled for 5CB on the waveguide structure. (c) Schematic diagram of the proposed molecular reorientation driven by strong surface anchoring during layer densification.
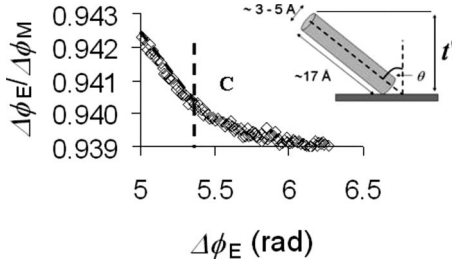
FIG. 10. Experimental perturbation rate ratio shown in the final region where the layer polar orientation becomes constant (region C). Extrapolation of the data from region B gives the chosen point of demarcation at $\Delta\phi_E=5.4$ rad. Inset: Proposed orientation and van der Waals surface dimensions of a surface bound 5CB molecule. The range of minor dimensions reflects uncertainty about the aliphatic chain relative orientation to the biphenyl ring system for molecules in different situations.

muthal and polar angles determined by the molecular scale surface roughness. During this stage, (experimental r values between 0.93 and 0.94 at the outset, where we attribute no special significance to these values) the layer is dilute and we cannot apply our theoretical treatment. We note only that for dilute layers the diluted refractive indices give smaller ratios than will be achieved at the condensed state. After this initial period a steady ratio value develops where r lies between 0.979 and 0.980. We demark the end of region A at $\Delta\phi_E \sim 0.8$ rad, at which point we suggest that there is a surface bound monolayer of liquid crystal molecules lying at some large average polar angle and weakly obscuring further surface binding sites to incoming molecules. The theoretical treatment [see Fig. 9(b)] gives a ratio of 0.979 for polar angles between 88° and 89°.

Using the arguments that follow, we can tentatively propose that this layer is one that comprises liquid crystal molecules lying at an average angle close to 90° but that the layer may not be as dense as can be achieved in the bulk liquid crystal.

The first exercise is to calculate the layer thickness at this point. It is known that, for layers that are not fully dense, thickness values calculated using values for the refractive index that assume the fully dense material are underestimates [6]. In the case of uniaxial systems it is nevertheless possible to quite accurately calculate the dense layer thickness using Eq. (19) where t_{TE} and t_{TM} are the calculated thicknesses obtained from the TE and TM phase changes:

$$t' = (t_{TM} + 2t_{TE})/3. \qquad (19)$$

Such calculations need make no assumptions about layer orientation and use the bulk isotropic refractive index given by

$$\langle n \rangle = \sqrt{(n_e^2 + 2n_0^2)/3}. \qquad (20)$$

We take the phase changes at the chosen position and calculate the effective indices that apply and then the thickness values that correspond to layers having the isotropic refractive index. The effective indices N_E and N_M are obtained through (for TE results)

$$\Delta\phi_E = k_0 l \Delta N_E = k_o l (N_E^0 + N_E), \qquad (21)$$

and similarly for TM results.

The material and waveguide parameters are those detailed in Sec. IV above. Using known parameters for the refractive index of 5CB, we have an isotropic refractive index, $\langle n \rangle$ =1.591 08. At the demarcation point, $\Delta\phi_E$=0.8106 rad and we require a thickness that corresponds to an effective index change ΔN_E of 6.803×10^{-6} (using window length l =12 mm and wavelength 0.6328 μm). Solving the four-layer waveguide problem gives t_{TE}=2.6 Å. Similarly, for the corresponding TM phase change, $\Delta\phi_M$=0.8274 rad, we obtain t_{TM}=2.4 Å, and thus the thickness value that would be representative of a fully dense layer is 2.57 Å.

The van der Waals dimensions of 5CB cannot be reconciled with such a small value [29]. The phenylene rings of the molecule are constrained to adopt a minimum torsion angle of 37°, and even if we propose that the cyanobiphenyl system is lying with its axis in the xz plane and that through van der Waals interactions with the surface the aliphatic tail is also induced to lie close to this plane (i.e., θ=90°) we cannot find a monolayer thickness that is less than 3 Å. If the tail is allowed to adopt its vacuum phase orientation, this thickness rises to 5 Å. Thus the indications are that at the point at which the experimental ratio begins to rise [Fig. 9(a)], we are unable to reliably apply an isotropic refractive index value [Eq. (20)] corresponding to the bulk liquid crystal. It appears, however, that the molecules are close enough to exert a mutual orientating force, as has been proposed for monolayers previously [30].

2. Region B

The experimental ratio rises through a maximum at around $\Delta\phi_E$=1.6 rad, at which point the experimental ratio is around 0.9845 and differs from the theoretical maximum value for a condensed layer (0.9811) by 3.4×10^{-3}. This experimental maximum ratio lies outside the range predicted using the bulk refractive index values and remains unexplained at present. Nevertheless, the shape of the experimental data progression is qualitatively similar to that of the theory and we might compare the two at the maximum point. The theory predicts a maximum in the ratio at a polar angle of 83°. The layer thickness by our definition (see Fig. 10, inset) would be given by $t' = 17 \cos(\theta) + w \sin(\theta)$, where w is the molecular minor dimension. Using the estimated molecular dimensions shown in the inset to Fig. 10, after taking account of the uncertainty in molecular minor dimensions, we expect a layer thickness of between 5 and 7 Å. Using the procedure detailed in the previous section, we can again calculate the expected condensed layer thickness. This gives an approximate thickness t'=5 Å. Once again there is a discrepancy, although smaller, which underestimates the expected thickness. The remainder of region B can be interpreted as a gradual reorientation of the layer upon densification. Additional molecules displace resident molecules to access the remaining surface sites and in doing so orient the layer by self-organization. This mechanism has been proposed before for molecules of 8CB densifying on rubbed polyamic acid layers [30,31].

According to the theoretical behavior of Fig. 5(b) such reorientation does not give curvature in the ratio versus angle until an angle of 43° is reached, where the ratio is around 0.90. The curvature seen in the experimental data beginning just after $\Delta\phi_E = 5$ rad (shown more clearly in Fig. 10) may therefore be attributed to the beginning of a second layer deposition. We therefore extrapolate the approximately linear region before this position to find the locus of the end point ratio for the monolayer. The demarcation point is thus chosen as $\Delta\phi_E = 5.3969$ radians ($\Delta\phi_M = 5.7398$ radians), at which point the experimental ratio is 0.9403 ± 0.0014, corresponding to an average polar angle of 56°. As an estimate of error, we note that $\pm 1°$ in the average polar angle corresponds to ± 0.002 in the expected ratio. Thus at this point, we propose a densified layer of 5CB molecules possessing this reduced average polar angle [32].

Using the bulk refractive index we once again calculate the condensed layer thickness at this point, which is $t' = 16.6 \pm 0.5$ Å. This compares with the geometrical values of between 12 and 14 Å. The experimentally determined thickness is this time *greater* than that predicted by the geometrical model and the polar angle inferred from the phase change ratio analysis. Although we can more readily understand measured thickness values that are larger, rather than smaller, than the minimum geometrical dimensions of the molecular model, we nevertheless explore what errors may arise from our qualitative choice of the demarcation point C. To arrive at a smaller thickness we would move this point back to somewhere before the onset of curvature. At $\Delta\phi_{TE} = 5$ rad, for example, we use the bulk index method to arrive at a layer thickness of 15.3 Å. The phase change ratio at this point ($r = 0.9422$) yields a polar angle of 57° and thus a geometrical thickness of between 11.8 and 13.5 Å. It would not seem justifiable to move the point further back than this and we conclude that there is an absolute thickness error of between 2.6 and 4.6 Å at the point we have chosen.

3. Region C

Further deposition beyond this point leads to a region where the experimental ratio flattens off. If we follow the argument from above, we might predict that a second, probably interdigitated, layer is forming and the effect of this is to increase the weighted average (combined layers) polar angle from the condensed monolayer value. The curvature in the ratio versus deposition is positive, indicating that any subsequent layer is oriented, at least initially, at an angle larger than 56°. The experimental and theoretical examination of such multilayers is the subject of our ongoing work. However, we tentatively propose that in the first stages of the growth of the second layer the molecules are lying almost flat, as was observed for the early stages of the monolayer. We apply a five layer model to the analysis and use the refractive indices and thickness found for the condensed monolayer as fixed parameters in the model. This then suggests that for the phase changes in the plateau region ($\Delta\phi_E = 6.4$ rad, $\Delta\phi_E = 6.8$ rad) the layer thickness is 2.4 Å, which is not inconsistent with some form of dilute layer lying in the plane. Despite this finding, there is overwhelming prior evidence that in the *condensed* state the second and third layers
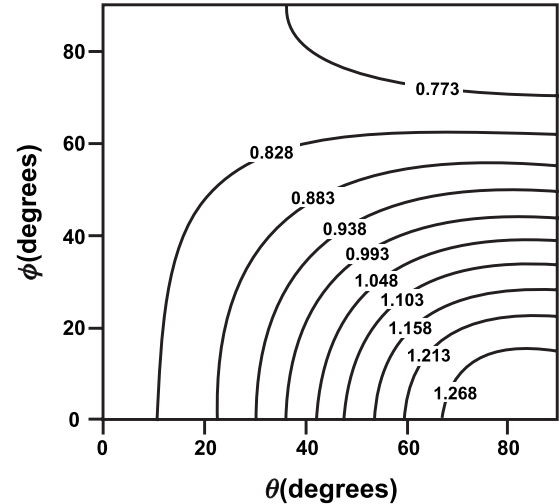

FIG. 11. Contour map for the perturbation rates ratio as a function of NLC polar and azimuthal angles.

of these liquid crystals, whether measured as spreading droplets or as evaporated thin films, are aligned at angles smaller than that of the first layer, and that interdigitation of the tails of the first and second layers is in part the cause of this alignment.

4. Discussion of thickness disagreements

Equations (19) and (20) indicate that the choice of refractive index value $\langle n \rangle$ influences the calculated layer thickness and that smaller values of refractive index would yield higher thickness values. Thus where, at the demarcation point at the end of region A, we have an underestimation of the thickness using this method, we can propose a layer that is not fully dense and thus has an index lower than that of the bulk liquid crystal. Correspondingly, in the region spanning the demarcation point between regions B and C we seem to have a thickness which is larger than that predicted by geometry and we must assume an index larger than the bulk liquid crystal. Regardless of what this means, the assumption of an index higher than that of the bulk liquid crystal would have the effect of reducing the calculated layer thickness by the methods of Eqs. (19) and (20) while simultaneously reducing the polar angle inferred from the experimental phase change ratios around this point, and thus increasing the geometrical layer thickness. We could expect much better agreement here if the index were allowed to be higher than that of the bulk liquid crystal.

VII. BIAXIAL SYSTEMS

The TE and TM perturbation rate ratio for nondegenerate NLC anchoring may also provide information about any preferential azimuthal alignment in these layers. Each measured ratio then is represented by pairs of polar and azimuthal angle possibilities. A plot is shown in Fig. 11 showing a number of ratios and their possible interpretations. Clearly, in most cases, it will be impossible to assign polar and azimuthal orientations but it is interesting to note that, as

the ratio increases above unity, the range of possible polar and azimuthal angles reduces.

Referring to Fig. 5(b), we note that for the present system any ratio value found between 0.81 and 0.99 could be interpreted equally in the uniaxial model as in this biaxial model. For example, the final experimental ratio at the condensed layer point on Fig. 10 ($r=0.94$) in the biaxial model occupies a pairwise range of angles (θ, ϕ) of approximately between (30,0) and (0,45). Such a situation, however, would require explanation based upon some preconditioning of the system if the uniaxial model was to be discounted. More usefully, however, for values of the ratio outside these uniaxial limits, the data would clearly point to some in-plane ordering of the molecules. The stronger the ordering, the more the ratio will be found in either the top or bottom right hand corners of the diagram of Fig. 11. Such ordering might be produced by rubbing, for instance, or by the oblique angle of deposition of an aligning layer, and would form an interesting extension to the present work.

VIII. CONCLUSIONS

We have observed the self-orientation, during densification, of a monolayer of the liquid crystal 5CB as it is condensed from the vapor phase onto a clean silicon oxynitride surface. The dual polarization interferometry method used is able to provide sufficient detail on the layer refractive indices that the average molecular polar angle evolution throughout the deposition path can be monitored in real time. Given the known refractive indices of this material and its known molecular dimensions, the data can be reliably interpreted. The deposition process proceeds in two steps: The first is the deposition of a precursor surface bound layer, possibly below full surface coverage, comprising molecules tilted at a large angle (effectively 90°) to the surface normal; the second stage is the insertion of further molecules in between the resident molecules, finding available surface binding sites and so displacing and reorienting the resident molecules. It is possible that the layer begins to behave as a liquid crystal exhibiting cooperative behavior at densities that are lower than in the bulk. The effect is to gradually align the molecules to a final condensed layer orientation of 56° from the surface normal. At this point there is reasonable agreement between theory and experiment, as would be expected for a fully condensed layer. These orientations and layer properties, when coupled with the absolute changes to the effective refractive indices that are produced, lead to layer thickness predictions that agree well with the molecular dimensions although some discrepancy in layer thickness is still observed. If this discrepancy is pointing to a problem with our choice of refractive index as input data then we should look for reasons to increase the refractive index of these surface

bound monolayers over and above that of the liquid state material.

We now turn to some of the problems encountered in previous studies in an attempt to clarify the large range of reported results. This first point to make is that we should not mix up interpretations on layer structure made from the spreading droplets [17,22] with those made from evaporated films [13,14]. Upon their reexamination of the monolayer regions of spreading droplets, the authors of [22] concluded that the monolayer region comprised molecules with the cyanobiphenyl ring axis system lying flat on the substrate. Such a situation would give rise to only a vanishingly small (interfacial) effect for second-order harmonic generation signals in the *p-p* polarization state and a zero signal in the *s-p* polarization state. Yet the authors of Ref. [13] find significant signals of both polarizations during the vapor deposition of 8CB molecules indicating the development of a monolayer with some polar axis orientation away from the plane. These signals grow monotonically with deposition time. Similarly there is a polar ordered layer interpretation of data for evaporated 5CB in [14]. This layer growth model is what we find here for vapor deposited 5CB. The spreading droplet monolayer structure is thus significantly different from that produced during vapor deposition and may, as proposed, represent a dilute system below a critical concentration at which correlated liquid crystal phase mutual orientation can take place, as we propose for the early stages of vapor deposition reported herein. Determining the thickness of such a dilute layer is problematic for all techniques, however. Ellipsometry is unable to reliably produce a monolayer thickness that does not require some rather special configurations of the molecules on the surface (8 Å for 8CB [22]) and x-ray modeling appears to contradict ellipsometry results (12 Å for 8CB [17]). In the case of DPI in the dilute regime, we have a small underestimation of feasible layer thickness and cannot improve on this without knowing precisely how dilute the layer is at this point. Even so, our study shows that we are inaccurate to only 1–2 Å or so of the layer thickness provided by completely flat lying molecules in this precursor stage of the monolayer.

The numerical method used that makes interpretations of the ratio of the effective index perturbation rates upon layer deposition is fully explained and is shown to provide a powerful way to extract data from anisotropic thin films provided optogeometrical data is known in advance.

ACKNOWLEDGMENTS

[1] G. H. Cross, Y. T. Ren, and N. J. Freeman, J. Appl. Phys. **86**, 6483 (1999).

[2] G. H. Cross, A. Reeves, S. Brand, M. J. Swann, L. L. Peel, N. J. Freeman, and J. R. Lu, J. Phys. D **37**, 74 (2004).

[3] S. M. Lin, C. K. Lee, Y. M. Wang, L. S. Huang, Y. H. Lin, S. Y. Lee, B. C. Sheu, and S. M. Hsu, Biosens. Bioelectron. **22**, 323 (2006).

[4] E. K. Mann, L. Heinrich, J. C. Voegel, and P. Schaaf, J. Chem. Phys. **105**, 6082 (1996).

[5] R. Horvath and J. J. Ramsden, Langmuir **23**, 9330 (2007).

[6] A. Mashaghi, M. Swann, J. Popplewell, M. Textor, and E. Reimhult, Anal. Chem. **80**, 3666 (2008).

[7] J. Li and S. T. Wu, J. Appl. Phys. **95**, 896 (2004).

[8] A. D. Price and D. K. Schwartz, Langmuir **22**, 9753 (2006).

[9] D. Demus, *Handbook of Liquid Crystals* (Wiley-VCH, Weinheim, 1998).

[10] F. J. Kahn, Appl. Phys. Lett. **22**, 386 (1973).

[11] S. Matsumoto, M. Kawamoto, and N. Kaneko, Appl. Phys. Lett. **27**, 268 (1975).

[12] C. S. Mullin, P. Guyot-Sionnest, and Y. R. Shen, Phys. Rev. A **39**, 3745 (1989).

[13] I. D. Olenik, K. Kocevar, I. Musevic, and T. Rasing, Eur. Phys. J. E **11**, 169 (2003).

[14] D. Taguchi, T. Manaka, and M. Iwamoto, Jpn. J. Appl. Phys., Part 1 **44**, 1037 (2005).

[15] M. P. Valignat, S. Villette, J. Li, R. Barberi, R. Bartolino, E. Dubois-Violette, and A. M. Cazabat, Phys. Rev. Lett. **77**, 1994 (1996).

[16] W. Chen, L. J. Martinez-Miranda, H. Hsiung, and Y. R. Shen, Phys. Rev. Lett. **62**, 1860 (1989).

[17] S. Bardon, R. Ober, M. P. Valignat, F. Vandenbrouck, A. M. Cazabat, and J. Daillant, Phys. Rev. E **59**, 6808 (1999).

[18] Y. G. J. Lau, R. M. Richardson, and R. Cubitt, J. Chem. Phys. **124**, 234910 (2006).

[19] M. T. Downton and M. P. Allen, Europhys. Lett. **65**, 48 (2004).

[20] M. T. Downton and S. Hanna, Europhys. Lett. **74**, 69 (2006).

[21] J. Z. Xue, C. S. Jung, and M. W. Kim, Phys. Rev. Lett. **69**, 474 (1992).

[22] L. Xu, M. Salmeron, and S. Bardon, Phys. Rev. Lett. **84**, 1519

[23] I. Musevic, R. Blinc, and B. Zeks, *The Physics of Ferroelectric and Antiferroelectric Liquid Crystals* (World Scientific, Singapore, 2000).

[24] G. H. Cross, A. A. Reeves, S. Brand, J. F. Popplewell, L. L. Peel, M. J. Swann, and N. J. Freeman, Biosens. Bioelectron. **19**, 383 (2003).

[25] C. K. Chen, P. Berini, D. Z. Feng, S. Tanev, and V. P. Tzolov, Opt. Express **7**, 260 (2000).

[26] Technical Note 001, "Essential Calibration Procedures for *Ana*Light® Instruments", http://www.farfield-group.com/infozone.asp

[27] A. Boudjemline, D. T. Clarke, N. J. Freeman, J. M. Nicholson, and G. R. Jones, J. Appl. Crystallogr. **41**, 523 (2008).

[28] We have observed in more rapid depositions and on hydrophobic surfaces in particular that there is a marked loss of contrast seen during the experiment. If the sample is simply left to settle for a period of a few hours, however, the contrast is restored. The implication is that scattering liquid crystal droplets spread over this period to give a uniform layer, possibly multiple molecules thick, but of a nonscattering nature and below the thickness that would cause the mode to couple out of the guiding layer. Reference [17,18] describe excellent measurements of such droplet spreading behavior.

[29] S. J. Clark, C. J. Adam, G. J. Ackland, J. White, and J. Crain, Liq. Cryst. **22**, 469 (1997).

[30] T. Shioda, Y. Okada, D. H. Chung, Y. Takanishi, K. Ishikawa, B. Park, and H. Takezoe, Jpn. J. Appl. Phys., Part 2 **41**, L266 (2002).

[31] T. Shioda, Y. Okada, Y. Takanishi, K. Ishikawa, B. Park, and H. Takezoe, Jpn. J. Appl. Phys., Part 1 **44**, 3103 (2005).

[32] We note in passing that our determination of the polar angle at 56° corresponds coincidentally to the "magic angle" shown by the intersection of the refractive index curves on Fig. 4. Without observing the trend in the ratio of Fig. 8 and without prior evidence from surface second harmonic generation studies that monolayers of *n*CB molecules on silica-like substrates had polar motifs, we would have to admit that an alternative interpretation of the layer geometry was that it was fully isotropic.

(2000).